International Journal of
MATERIALS RESEARCH

Zeitschrift für METALLKUNDE

Original Contributions

Jun Cai[a], Jiamin Shi[a], Kuaishe Wang[a], Fuguo Li[b], Wen Wang[a], Qingjuan Wang[a], Yingying Liu[a]

[a] School of Metallurgical Engineering, Xi'an University of Architecture and Technology, Xi'an, P.R. China
[b] School of Materials Science and Engineering, Northwestern Polytechnical University, Xi'an, P.R. China

A modified parallel constitutive model for elevated temperature flow behavior of Ti-6Al-4V alloy based on multiple regression

Constitutive analysis for hot working of Ti-6Al-4V alloy was carried out by using experimental stress–strain data from isothermal hot compression tests. A new kind of constitutive equation called a modified parallel constitutive model was proposed by considering the independent effects of strain, strain rate and temperature. The predicted flow stress data were compared with the experimental data. Statistical analysis was introduced to verify the validity of the developed constitutive equation. Subsequently, the accuracy of the proposed constitutive equations was evaluated by comparing with other constitutive models. The results showed that the developed modified parallel constitutive model based on multiple regression could predict flow stress of Ti-6Al-4V alloy with good correlation and generalization.

Keywords: Ti-6Al-4V alloy; Modified parallel constitutive model; Constitutive equations; Flow stress; High temperature flow behavior

1. Introduction

Ti-6Al-4V alloy as a representative of the $\alpha + \beta$ type titanium alloy has distinctive characteristics including high mechanical properties, elevated corrosion resistance, and low density, which makes it an ideal material in the surgical, aviation, aerospace, automotive and marine industries [1–3]. Therefore, great attention has been paid in the scientific literatures to investigating the deformation behavior of this alloy [4–9].

Recently, numerical simulation technology such as the finite element method (FEM) has been widely applied to the investigation of metal deformation, and the accuracy of constitutive equations is the key to improve the reliability of the numerical simulation [10]. Meanwhile, the constitutive equation is an effective method to describe flow behavior of metal alloys, and enables researchers to present the basic function of flow stress and hot processing parameters (including deformation temperature, strain rate, and strain) [11]. Therefore, it is of vital significance to obtain an accurate constitutive equation between the flow stress and deformation parameters. About the constitutive equations for Ti-6Al-4V alloy, researchers have published many works, including physical, phenomenological, and artificial neural network (ANN) models. Kotkunde et al. [12] investigated the flow behavior of Ti-6Al-4V alloy by using four constitutive models: modified Johnson–Cook, modified Arrhenius type, modified Zerilli–Armstrong and Rusinek–Klepaczko models. Luo et al. studied the high temperature flow behavior of Ti-6Al-4V alloy by internal state variables [13] and fuzzy neural network [14]. Picu and Majorell [15] proposed a physically-based model to describe the deformation mechanisms of Ti-6Al-4V alloy. Zhang et al. [16] proposed the Arrhenius and Norton–Hoff constitutive mod-

els to characterize the tensile behavior of Ti-6Al-4V alloy. On the basis of an orthogonal experiment and variance analysis, Xiao et al. [17] proposed a constitutive model to describe the elevated temperature flow behavior of TiNiNb alloy. However, this constitutive model ignores the combined effect of influence factors on flow stress, which decreases the accuracy of the constitutive equation. Then, a double multiple nonlinear regression method (DMNR) with higher accuracy was proposed by Yuan et al. [18] to predict the flow stress of Ti-6Al-4V alloy. However, the DMNR model is very complex, and the time required for evaluating these material constants involved in the DMNR constitutive model is also very long.

An ideal constitutive model should involve a reasonable number of material constants, which can be evaluated from a limited amount of experimental data, and should be able to reflect the flow stress with adequate accuracy and reliability [19]. Therefore, the objective of this study is to establish a suitable constitutive model predict the high temperature flow behavior of Ti-6Al-4V alloy in both $\alpha + \beta$ phase and single β phase regions. For this purpose, isothermal hot compression tests were conducted in the temperature range of 1 073 – 1 223 K and a strain rate range of 0.0005 – 1 s^{-1} on a Gleeble-3500 simulator. On the basis of the effect of strain, strain rate and deformation temperature on the flow stress, a modified parallel constitutive model (MPCM) based on multiple regression was proposed. Thereafter, comparative analysis between calculated and experimental results was performed to verify the proposed constitutive model. Finally, the accuracy of the proposed constitutive equation was evaluated by comparing with other constitutive models.

2. Experimental details

The chemical composition (wt.%) of Ti-6Al-4V alloy investigated in the present study is given in Table 1. The original microstructure of as-received Ti-6Al-4V alloy is shown in Fig. 1, and consists of equiaxed primary α phase (hexagonal close-packed) and intergranular β phase (body-centered cubic). The β transus temperature of Ti-6Al-4V alloy is about 1 236 K.

As is well known, compression testing and tensile testing are the two most common used methods to understand the deformation behavior of metals. Yielding strength, fracture strength, reduction of area and elongation of metal materials can be obtained from tensile testing. For titanium alloys, high temperature tensile tests are often employed at lower strain rates [20 – 23]. Particularly, superplastic behavior can be investigated by high temperature tensile testing, such as Ti-6Al-4V alloy [24 – 26], TA15 titanium alloy [27], Ti600 alloy [28], Ti-6.4Al-2.6Mo-1.5Cr-0.4Fe-0.3Si alloy [29], and so on. However, compression tests can be performed over a wide range of strain rates, even at a strain rate of 100 s^{-1} [30]. Therefore, isothermal compression tests are used in this research. It is well known that the main deformation temperature range for Ti-6Al-4V alloy is located in the $\alpha + \beta$ phase region, and in processes such as hot die forging [31, 32], isothermal forging [33, 34], and superplastic forming [35, 36]. Therefore, four temperatures (1 073, 1 123, 1 173 and 1 223 K) are chosen in the $\alpha + \beta$ phase region, and two temperatures (1 273 and 1 323 K) are chosen in the single β phase region.

Cylindrical specimens with a diameter of 8 mm and a height of 12 mm were prepared for hot compression tests. In order to obtain uniform temperature, each specimen was heated to the deformation temperature at a rate of 10 K s^{-1}, and held for 5 min at the isothermal conditions before compression tests. Then isothermal compression tests were carried out in the strain rate range of 0.001 – 1 s^{-1} and the temperatures range of 1 073 – 1 323 K in a Gleeble-3500 simulator. After deformation, the specimens were quenched in water, and the stress–strain curves were recorded automatically during isothermal compression process. The experiment was carried out once under each deformation condition.

3. Results and discussion

3.1. Flow stress

The flow stress curves acquired through hot compression tests are given in Fig. 2 and exhibit similar results to those of Luo et al. (1 273 K) [1] and Seshacharyulu et al. (1 123 K) [30]. It can be seen from the curves that the flow stress is sensitively dependent on deformation temperature and strain rate. The flow stress increases with the increase of the strain rate at a curtain temperature, and increases with the decrease of the temperature at a curtain strain rate. At the initial stage, the flow stress increases rapidly with the increase of strain, owing to dislocation generation and multiplication becoming significant with the increase of deformation, resulting in obvious work hardening. Meanwhile, the dynamic softening (DS) caused by cross-slip during this period is not enough to overcome the effect of work hardening. Therefore, the flow stress quickly increases. Then, with the increase of deformation, a peak stress appears, and flow

Table 1 Chemical composition of as-received Ti-6Al-4V billet.

Main component (wt.%)			Impurities (wt.%)			
Al	V	Ti	Fe	C	H	O
6.02	3.78	Balance	0.08	0.007	0.0082	0.074

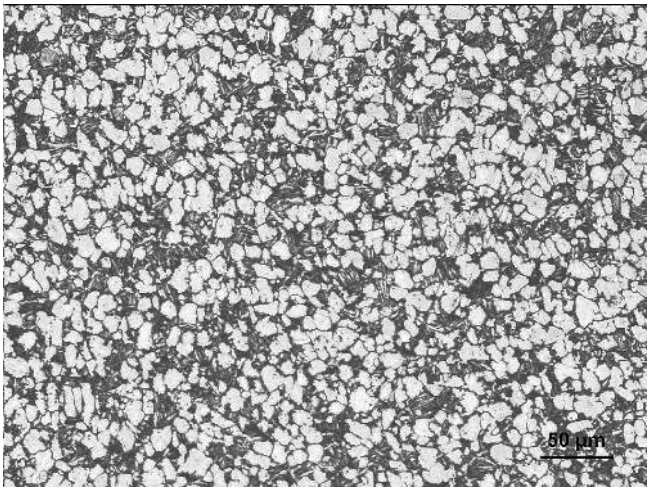

Fig. 1. The microstructure of the as-received Ti-6Al-4V alloy.

stress continuously decreases to a steady value due to the DS is sufficient to counteract the effect of work hardening.

In addition, it should be noted that the flow stress exhibits a significant serrated oscillation at the strain rate of 1 s^{-1}, which is more obvious with the increase of deformation temperature. Similar oscillations were also observed for Ti17 alloy [37], TC21 alloy [38, 39], and Ti-6.5Al-2Sn-4Zr-4Mo-1W-0.2Si titanium alloy [40]. The main reason for this serrated oscillation phenomenon can be attributed to the indication of instability, such as flow localization or cracking [41]. Meanwhile, it can be observed in Fig. 2 that the DS effect in the $\alpha + \beta$ phase region is more obvious than that in single β phase region. The noticeable softening phenomenon at lower deformation temperatures

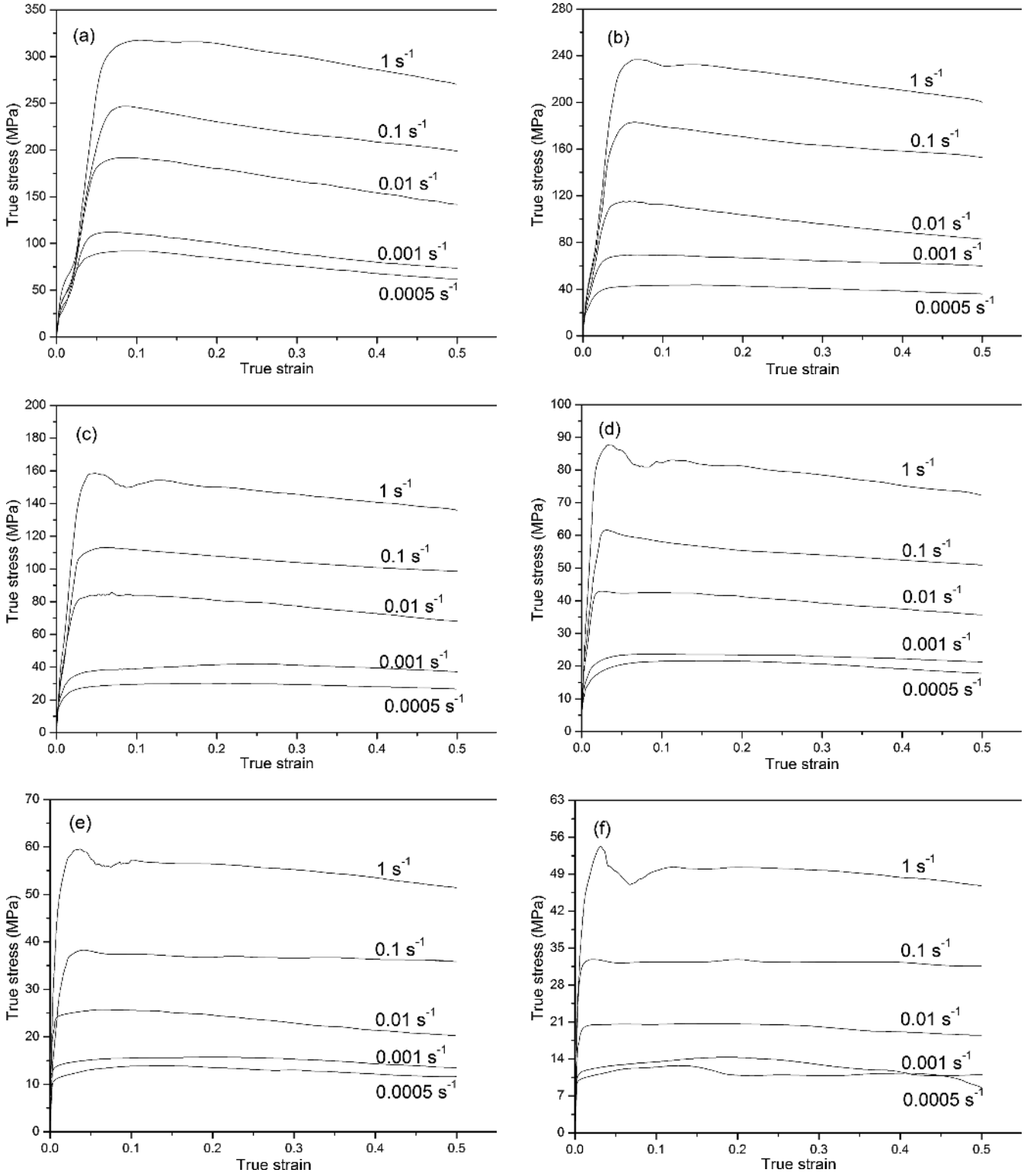

Fig. 2. Flow curves of Ti-6Al-4V alloy at various strain rates at temperatures of: (a) 1 073 K, (b) 1 123 K, (c) 1 173 K, (d) 1 223 K, (e) 1 273 K, and (f) 1 323 K.

may be attributed to deformation heating which raises the actual temperature of the specimens [42].

Figure 3 demonstrates the influence of deformation temperature and strain rate on the peak stress and the steady stress ($\varepsilon = 0.5$) during the isothermal compression of Ti-6Al-4V alloy. From Fig. 3, it can be seen that the deformation temperature has a significant influence on the peak stress and the steady stress below 1 223 K ($\alpha + \beta$ phase region), but the effect of deformation temperature becomes slight above 1 223 K (single β phase region). This phenomenon results from the microstructural evolution during the elevated temperature deformation. In the $\alpha + \beta$ phase region, the content of α phase decreases with the increase of deformation temperature, leading to an obvious decrease in peak and steady stress [30]. In the single β phase region, the peak stress and the steady stress exhibit temperature dependence owing to the fact that the β phase becomes the continuous phase.

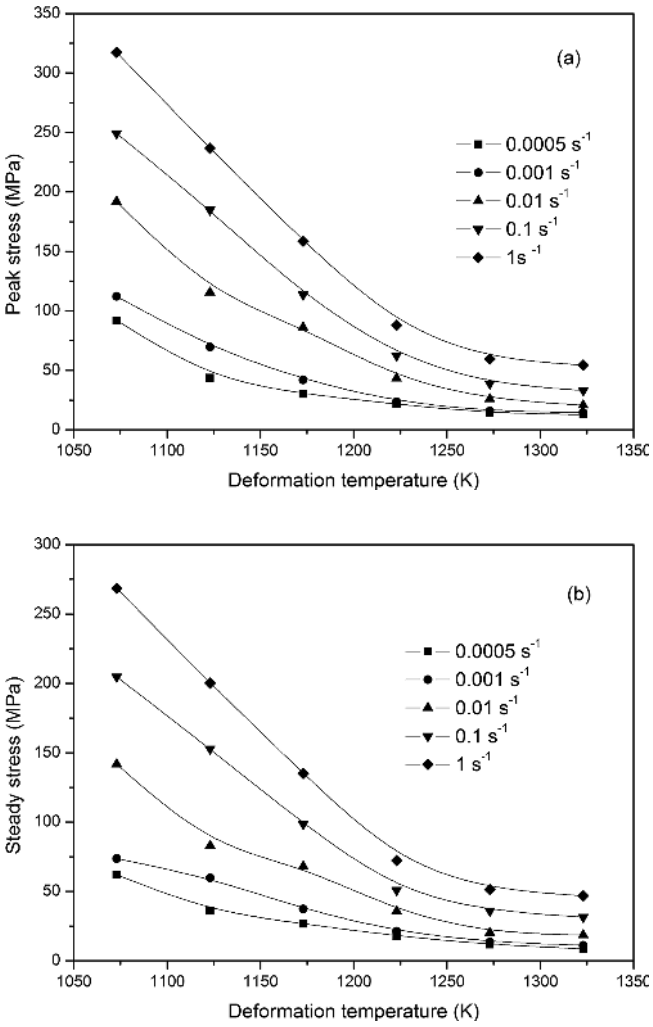

Fig. 3. Peak stress and steady stress curves of Ti-6Al-4V alloy during elevated temperature deformation: (a) Peak stress; (b) Steady stress ($\varepsilon = 0.5$).

3.2. Constitutive equation

The high temperature flow behavior of Ti-6Al-4V alloy represented by the constitutive equation consists of flow stress and influence parameters. Figure 4 gives the relationship between the flow stress and influence parameters. x_i ($i = 1, 2, 3, \ldots, n$) are the test factors; h_j ($j = 1, 2, 3, \ldots, m$) are the analysis factors; y is the objective function representing the flow stress, and y is a pan-function of x_i and h_j, $y = F[h_1, h_2, \ldots, h_m] = f(x_1, x_2, \ldots, x_n)$; ω_j are the converged weights, which represent the contribution of analysis factors h_j to objective function y. The analysis factors h_j are the functions of test factors x_i. Therefore, the objective function y can be obtained from the contribution functions $f[h_j]$ and the converged weights ω_j. Non-linear regression based on the experimental data is employed to acquire the contribution function that defines the relationship between analysis factors h_j and objective function y (described as

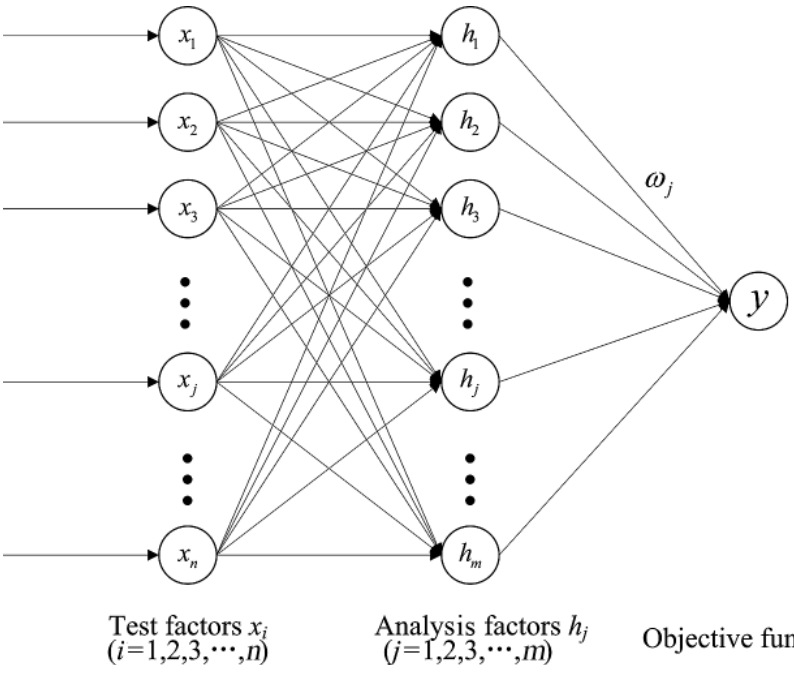

Fig. 4. Relationship between the flow stress and influence parameters.

$f_j = f[h_j]$). The converged weights ω_j can be acquired by using the multivariate non-linear regression based on a least squares algorithm.

In order to acquire the constitutive equation for the elevated temperature deformation behavior of Ti-6Al-4V alloy, independent factors strain, strain rate, and deformation temperature are defined as the test factors x_i. The analysis factors are strain, strain rate and deformation temperature, as shown in Eq. (1).

$$\begin{aligned} h_1(x_1) &= \varepsilon \\ h_2(x_2) &= \dot{\varepsilon} \\ h_3(x_3) &= 1/T \end{aligned} \tag{1}$$

where ε is strain, $\dot{\varepsilon}$ is strain rate (s^{-1}), T is absolute deformation temperature (K). After determination of all the analysis factors mentioned above, taking the mean flow stress values of each analysis factor, the contribution functions f_j can be obtained by using the non-linear regression, where

$$\begin{aligned} f_1 &= f_\varepsilon[h_1(x_1)] \\ f_2 &= f_{\dot{\varepsilon}}[h_2(x_2)] \\ f_3 &= f_T[h_3(x_3)] \end{aligned} \tag{2}$$

After the determination of all the contribution functions f_j mentioned above, the constitutive equation can be obtained. During hot deformation, the constitutive equation of metals can be expressed as:

$$\sigma = f(\varepsilon, \dot{\varepsilon}, T, C, S) \tag{3}$$

where C is for the chemical composition of material, and S is for the microstructure of material. However, composition will not change during the deformation. Meanwhile, the material microstructure reflects the deformation state in its current deformation condition, and it changes consistent with the deformation condition [18]. Therefore, the parameter S can also be neglected, and Eq. (3) can be simplified as:

$$\sigma = f(\varepsilon, \dot{\varepsilon}, T) \tag{4}$$

The effect of strain, strain rate and deformation temperature on the flow stress can be expressed in another form as [17]:

$$\sigma = \sigma_0 f_\varepsilon f_{\dot{\varepsilon}} f_T \tag{5}$$

where σ_0 is the initial stress of Ti-6Al-4V alloy under current experimental conditions; f_ε, $f_{\dot{\varepsilon}}$ and f_T are the influence coefficients of the strain, strain rate and deformation temperature, respectively. Then, Eq. (5) can be simplified as Eq. (6):

$$\sigma = f_0 \cdot f_1 \cdot f_2 \cdot f_3 \tag{6}$$

where $f_0 = \sigma_0$, $f_1 = f_\varepsilon$, $f_2 = f_{\dot{\varepsilon}}$, $f_3 = f_T$. Therefore, Eq. (6) can be termed a parallel constitutive model. Taking natural logarithms of both sides of Eq. (6), Eq. (7) can be obtained as follows:

$$\ln\sigma = \ln f_0 + \ln f_1 + \ln f_2 + \ln f_3 \tag{7}$$

It can be seen from Eq. (5) to Eq. (7) that the coupled effects between the deformation parameters are neglected in the original parallel constitutive model, which may decrease the accuracy of the constitutive equation. In the DMNR model, seven contribution functions (f_0, f_ε, $f_{\dot{\varepsilon}}$, f_T, $f_{\varepsilon-\dot{\varepsilon}}$, $f_{\dot{\varepsilon}-T}$ and $f_{\varepsilon-T}$) are employed to describe the independent effects of variables (strain, strain rate and temperature) and their combined effects [18], which result in the equation being too complex. Meanwhile, the contribution functions of combined effects ($f_{\varepsilon-\dot{\varepsilon}}$, $f_{\dot{\varepsilon}-T}$ and $f_{\varepsilon-T}$) can be divided into f_ε, $f_{\dot{\varepsilon}}$ and f_T. Therefore, the converged weights ω_j can be used to describe the combined effects. Considering the converged weights ω_j, the following expression can be derived:

$$\ln\sigma = \ln f_0 + \omega_1 \ln f_1 + \omega_2 \ln f_2 + \omega_3 \ln f_3 \tag{8}$$

Then Eq. (8) can be rewritten as:

$$\ln\sigma = \ln f_0 + \sum_{j=1}^{3} \omega_j \ln f_j \tag{9}$$

Then, the obtained modified parallel constitutive equation can be expressed as:

$$\sigma = f_0 \cdot {f_1}^{\omega_1} \cdot {f_2}^{\omega_2} \cdot {f_3}^{\omega_3} = f_0 \prod_{j=1}^{3} {f_j}^{\omega_j} \tag{10}$$

As for Ti-6Al-4V alloy, the modified parallel constitutive equation is given as:

$$\sigma = f_0 \cdot {f_\varepsilon}^{\omega_1} \cdot {f_{\dot{\varepsilon}}}^{\omega_2} \cdot {f_T}^{\omega_3} \tag{11}$$

3.3. Determination of the contribution functions and converged weights

The mean flow stress values $\bar{\sigma}$ are employed to obtain the modified parallel constitutive equation. $\bar{\sigma}_\varepsilon$ is the mean value of flow stress at all temperatures and strain rates, $\bar{\sigma}_{\dot{\varepsilon}}$ is the flow stress at all temperatures and strain, and $\bar{\sigma}_T$ is the flow stress at all strain and strain rate. K_ε, $K_{\dot{\varepsilon}}$, and K_T are the levels of strain, strain rate, and deformation temperature, as given in Eq. (12):

$$\begin{aligned} \bar{\sigma}_\varepsilon &= \sum_{T-\dot{\varepsilon}} \sigma/(K_T \cdot K_{\dot{\varepsilon}}) \\ \bar{\sigma}_{\dot{\varepsilon}} &= \sum_{T-\varepsilon} \sigma/(K_T \cdot K_\varepsilon) \\ \bar{\sigma}_T &= \sum_{\varepsilon-\dot{\varepsilon}} \sigma/(K_\varepsilon \cdot K_{\dot{\varepsilon}}) \end{aligned} \tag{12}$$

In this research, the values of strain are selected in the range of 0.1–0.8 at an interval of 0.1, the strain rates are chosen as 0.0005 s^{-1}, 0.001 s^{-1}, 0.01 s^{-1}, 0.1 s^{-1}, and 1 s^{-1}, and temperatures are selected as 1 073–1 323 K at an interval of 50 K. Therefore, the values of K_ε and $K_{\dot{\varepsilon}}$ are 8 and 5 respectively. The values of K_T in the $\alpha + \beta$ phase and single β phase are 4 and 2 respectively. Figure 5 demonstrates the relationship between $\bar{\sigma}_\varepsilon$ and ε. It can be seen from Fig. 5 that a linear fit and a parabolic spline can be employed to express the relationship between $\bar{\sigma}_\varepsilon$ and ε in $\alpha + \beta$ phase (Eq. (13)) and single β phase (Eq. (14)).

$$\bar{\sigma}_\varepsilon = 27.91294 + 0.77074\varepsilon - 13.62222\varepsilon^2 \tag{13}$$

$$\bar{\sigma}_\varepsilon = 117.27678 - 49.93901\varepsilon \tag{14}$$

Figure 6 gives the relationship between $\ln(\bar{\sigma}_{\dot{\varepsilon}})$ and $\ln(\dot{\varepsilon})$, and a linear fit is employed to express the relationship between $\ln(\bar{\sigma}_{\dot{\varepsilon}})$ and strain $\ln(\dot{\varepsilon})$ in the α + β phase and single β phase respectively, as shown in Eq. (15) (α + β phase) and Eq. (16) (single β phase).

$$\ln(\bar{\sigma}_{\dot{\varepsilon}}) = 5.3089 + 0.19339 \ln \dot{\varepsilon} \tag{15}$$

$$\ln(\bar{\sigma}_{\dot{\varepsilon}}) = 3.96334 + 0.19432 \ln \dot{\varepsilon} \tag{16}$$

Therefore, it can be obtained from Eq. (15) and Eq. (16) that the mean values of strain rate sensitivity exponent m of Ti-6Al-4V alloy are 0.19339 in α + β phase and 0.19432 in single β phase. Figure 7 gives the relationship between $\ln(\bar{\sigma}_T)$ and 1 000/T, and a linear fit can be used to describe the relationship between $\ln(\bar{\sigma}_T)$ and 1 000/T in α + β phase and single β phase respectively, as shown in Eq. (17) (α + β phase) and Eq. (18) (single β phase).

$$\ln(\bar{\sigma}_T) = -5.83332 + \frac{11.84193 \times 10^3}{T} = -5.83332 + \frac{0.19339 \times 509.09 \times 10^3}{RT} \tag{17}$$

$$\ln(\bar{\sigma}_T) = -0.04849 + \frac{4.32166 \times 10^3}{T} = -0.04849 + \frac{0.19432 \times 184.9 \times 10^3}{RT} \tag{18}$$

where R is the universal gas constant (8.314 J mol^{-1} K^{-1}). Andd

$$Q = \frac{R}{m} \frac{\mathrm{d} \ln \sigma}{\mathrm{d}(1/T)} \tag{19}$$

Therefore, it can be found from Eqs. (17) and (18) that the values of average apparent activation energy Q for Ti-6Al-4V alloy are 509.09 kJ mol^{-1} for α + β phase and 184.9 kJ mol^{-1} for single β phase, which are very close to those obtained from Eq. (20) (500.60 kJ mol^{-1} for α + β phase and 197.60 kJ mol^{-1} for single β phase).

$$Q = Rn \frac{\mathrm{d}\{\ln[\sinh(\alpha\sigma)]\}}{\mathrm{d}(1/T)} \tag{20}$$

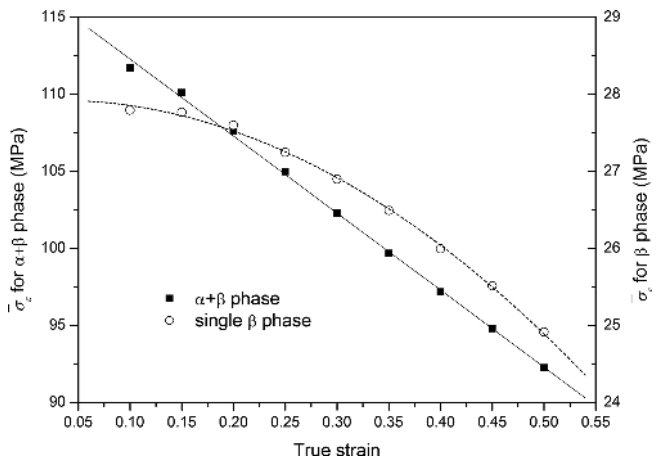

Fig. 5. Relationship between $\bar{\sigma}_{\varepsilon}$ and ε.

where α and n are material constants. It has been widely acknowledged that the microstructural evolution is controlled by the thermal activation, and the DS behavior of metal materials during hot deformation can be identified through comparison between the activation energy Q and the self-diffusion activation energy Q_s [43]. DRV is associated with dislocation climbing and cross-slipping for dislocation rearrangement and elimination, which is diffusion-controlled [44]. Therefore, the value of activation energy Q for DRV is close to the value of Q_s. DRX is characterized by the non-distortion subgrain nucleation and high-angle boundaries directional migration, which results in the higher level of Q [45]. Thus, a simple criterion can be introduced to identify the DS behavior during hot deformation by comparing the values of Q and Q_s [46]:

$$\begin{cases} Q > Q_s \Rightarrow \text{DRX} \\ Q \approx Q_s \Rightarrow \text{DRV} \end{cases} \tag{21}$$

The values of Q_s for pure α-titanium and β-titanium alloys have been determined to be 242 kJ mol^{-1} [47] and 153 kJ mol^{-1} [48] respectively. Therefore, the values of

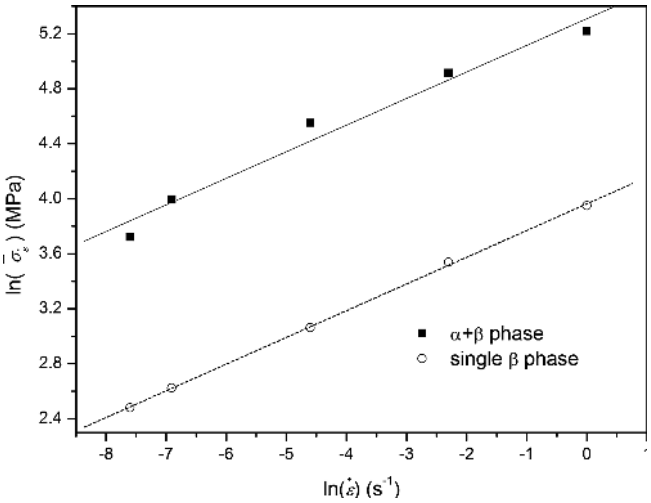

Fig. 6. Relationship between $\ln(\bar{\sigma}_{\dot{\varepsilon}})$ and $\ln(\dot{\varepsilon})$.

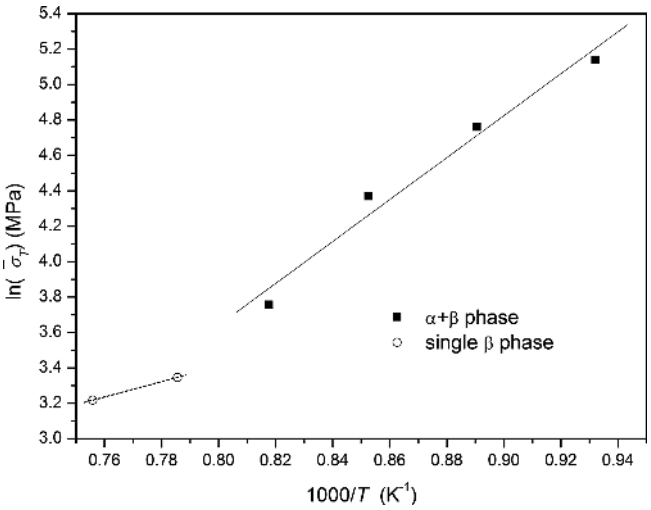

Fig. 7. Relationship between $\ln(\bar{\sigma}_T)$ and 1 000/T.

average apparent activation energy Q in both α + β phase and single β phase are higher than those of Q_s, which indicate that DRX may occur in α + β phase and single β phase. Meanwhile, it should be noted that lack of deformation time may result in insufficient diffusion in preparation for polygonization where DRX nucleates [49]. Therefore, the strain rate also has influence on the dynamic softening process. Taking slopes between the adjacent two points of strain rate in Fig. 6, the relationship between m and strain rate can be obtained, as illustrated in Fig. 8.

It can be found from Fig. 8 that the value of m in α + β phase decreases with increasing strain rate, the maximum value of m is about 0.393, and the minimum value is about 0.158. The maximum and the minimum values of m in single β phase are 0.207 and 0.178 respectively. Eq. (22) shows strain rate sensitivity exponent m maintains a steady value of 0.2 under steady-state deformation undergoing DRV [49]:

$$\sigma^5 = A \cdot \dot{\varepsilon} \cdot \exp(Q/RT) \tag{22}$$

Therefore, from Eq. (21), Eq. (22), Fig. 7 and Fig. 8, DRX can occur at lower strain rate. Figure 9 shows the microstructure of Ti-6Al-4V alloy deformed under various deformation conditions. The fine equiaxed DRX grains can be found from Fig. 9a (strain rate of 0.001 s^{-1} and deformation

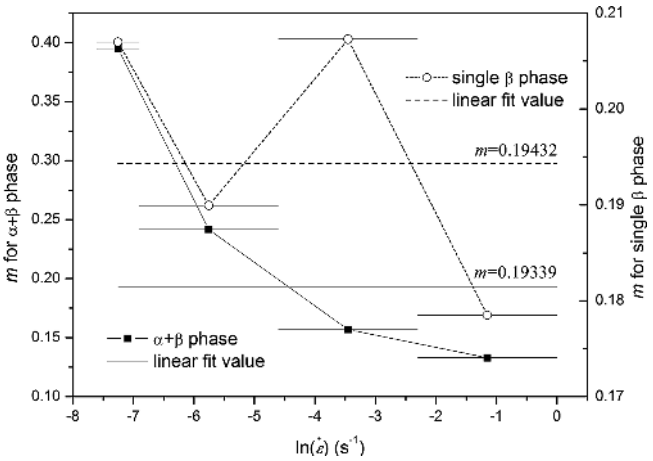

Fig. 8. Relationship between m and $\ln(\dot{\varepsilon})$.

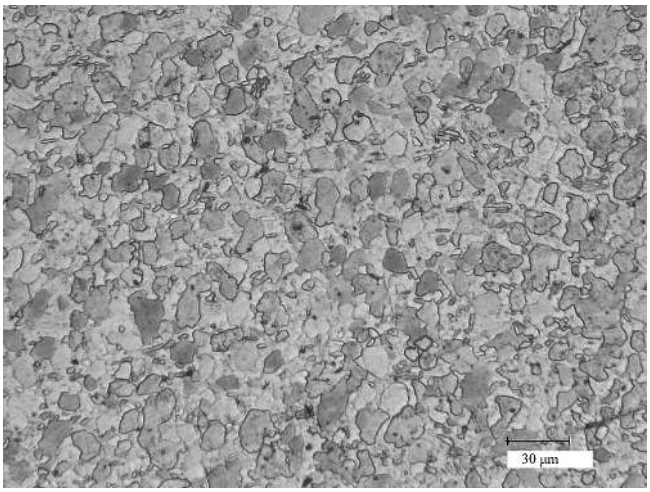

(a)

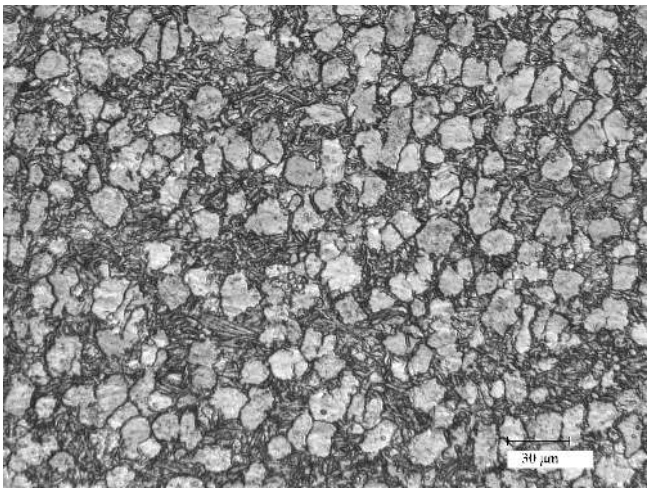

(b)

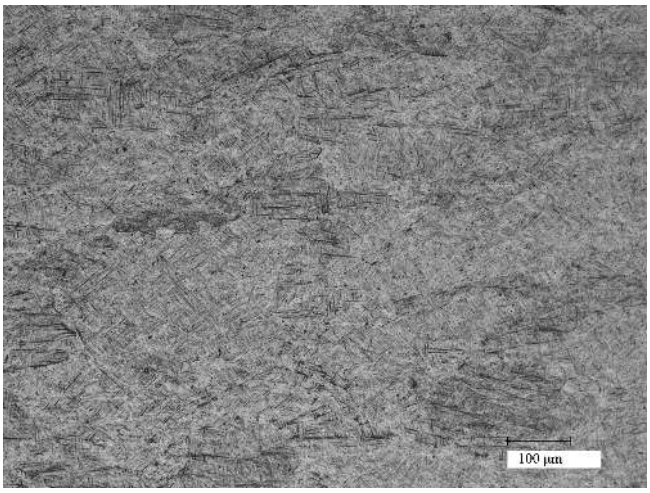

(c)

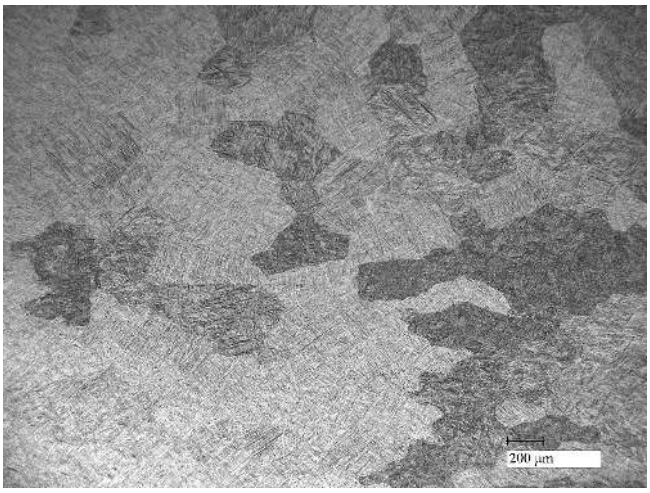

(d)

Fig. 9. Microstructures of Ti-6Al-4V alloy deformed under various deformation conditions: (a) strain rate of 0.001 s^{-1} and temperature of 1 173 K; (b) strain rate of 1 s^{-1} and temperature of 1 173 K; (c) strain rate of 1 s^{-1} and temperature of 1 273 K; (d) strain rate of 0.0005 s^{-1} and temperature of 1 323 K.

temperature of 1 173 K). However, at higher strain rate of α + β phase, no obvious DRX grains can be observed, as shown in Fig. 9b. In Fig. 9c, a typical coarse Widmanstätten structure consisting of primary β grains can be clearly observed, which indicates the unstable deformation under these deformation conditions (strain rate of 1 s^{-1} and deformation temperature of 1 273 K). DRX β grains can be observed at lower strain rate, as illustrated in Fig. 9d. A similar result was also reported by Honarmandi and Aghaie-Khafri [50] that DRX occurs at 0.001 s^{-1} in single β phase. Meanwhile, the apparent activation energy Q was calculated as 168.5 kJ mol^{-1} by Honarmandi and Aghaie-Khafri [50].

Equation (6) is rewritten as:

$$f_\varepsilon f_{\dot\varepsilon} f_T = \frac{\sigma}{\sigma_0} \tag{23}$$

Equation (13) to Eq. (18) are used to regress the equations of f_ε, $f_{\dot\varepsilon}$ and f_T. Based on Eq. (23), the values of f_ε at various strain can be obtained from $\bar\sigma_\varepsilon/\bar\sigma_0$, and $\bar\sigma_0$ is the value of $\bar\sigma_\varepsilon$ at the minimum level of each factor (i. e. strain 0.1, strain rate 0.0005 s^{-1}, and temperature 1 073 K in this study), as shown in Table 2 and Table 3.

A linear fit (Eq. (24)) and a parabolic fit (Eq. (25)) are found to represent the relationship between f_ε and ε with a good correlation and generalization for α + β phase and single β phase respectively, as shown in Fig. 10a.

$$f_\varepsilon = 1.04448 - 0.4447\varepsilon \tag{24}$$

$$f_\varepsilon = 1.00222 + 0.02773\varepsilon - 0.48905\varepsilon^2 \tag{25}$$

Table 2. Regression of f_ε in α + β phase.

ε	$\bar\sigma_\varepsilon$ (MPa)	$f_\varepsilon = \bar\sigma_\varepsilon/\bar\sigma_0$
0.10	112.28	1.0000
0.15	109.79	0.9778
0.20	107.29	0.9555
0.25	104.79	0.9333
0.30	102.30	0.9111
0.35	99.80	0.8888
0.40	97.30	0.8666
0.45	94.80	0.8444
0.50	92.31	0.8221

Table 3. Regression of f_ε in single β phase.

ε	$\bar\sigma_\varepsilon$ (MPa)	$f_\varepsilon = \bar\sigma_\varepsilon/\bar\sigma_0$
0.10	27.85	1.0000
0.15	27.72	0.9954
0.20	27.52	0.9882
0.25	27.25	0.9786
0.30	26.92	0.9665
0.35	26.51	0.9520
0.40	26.04	0.9351
0.45	25.50	0.9157
0.50	24.89	0.8938

Likewise, the expressions of contribution functions $f_{\dot\varepsilon}$ and f_T for α + β phase are acquired as follows:

$$f_{\dot\varepsilon} = \exp(1.46987 + 0.19338\ln\dot\varepsilon) \tag{26}$$

$$f_T = \exp\left(-11.03657 + 11.84226 \times \frac{1\,000}{T}\right) \tag{27}$$

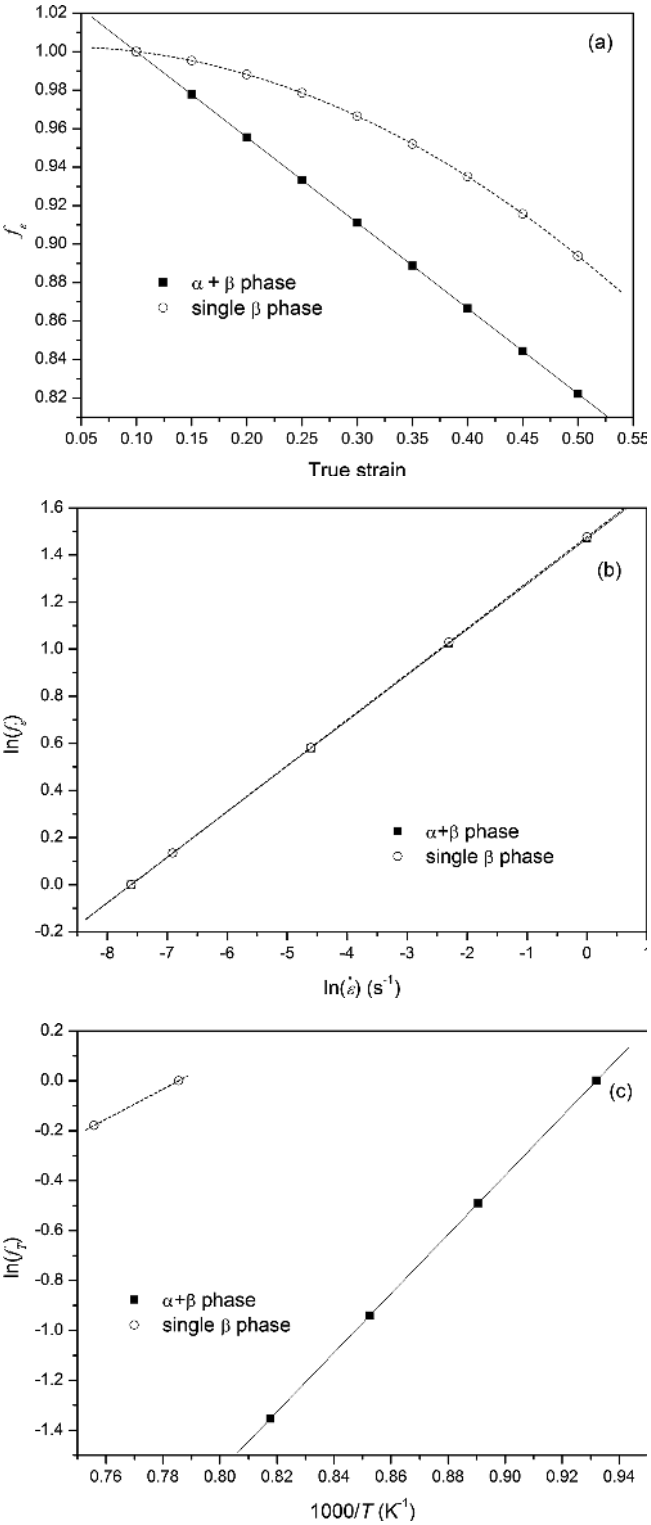

Fig. 10. Relationship between (a) f_ε and ε; (b) ln($f_{\dot\varepsilon}$) and ln($\dot\varepsilon$); (c) ln(f_T) and 1 000/T.

Meanwhile, the formulas of $f_{\dot{\varepsilon}}$ and f_T for single β phase are given as follows:

$$f_{\dot{\varepsilon}} = \exp(1.47674 + 0.1943 \ln \dot{\varepsilon}) \tag{28}$$

$$f_T = \exp\left(-4.74286 + 6.03766 \times \frac{1\,000}{T}\right) \tag{29}$$

The relationships between $\ln(f_{\dot{\varepsilon}})$ and $\ln(\dot{\varepsilon})$ as well as $\ln(f_T)$ and $1\,000/T$ are given in Fig. 10b and c.

Owing to the fact that multivariate regression analysis is a highly flexible system for examining the relationship between a collection of independent variables and a dependent variable, the correction coefficient f_0 and the converged weights ω_j can be obtained by least-squares regression with the independent variables $\ln(f_\varepsilon)$, $\ln(f_{\dot{\varepsilon}})$, $\ln(f_T)$ and the dependent variable $\ln(\sigma)$ obtained in this experiment. Through the multivariate regression test, the values of f_0 and ω_j are acquired and listed in Table 4.

Therefore, the developed modified parallel constitutive model of Ti-6Al-4V alloy during hot working based on multiple regression can be summarized as Eq. (30) (α + β phase) and Eq. (31) (single β phase).

$$\begin{cases} \sigma = f_0 \cdot {f_\varepsilon}^{0.9799} \cdot {f_{\dot{\varepsilon}}}^{1.006} \cdot {f_T}^{0.996} \\ f_0 = 86.57 \\ f_\varepsilon = 1.04448 - 0.4447\varepsilon \\ f_{\dot{\varepsilon}} = \exp(1.46987 + 0.19338 \ln \dot{\varepsilon}) \\ f_T = \exp\left(-11.03657 + 11.84226 \times \frac{1\,000}{T}\right) \end{cases} \tag{30}$$

$$\begin{cases} \sigma = f_0 \cdot {f_\varepsilon}^{1.312} \cdot {f_{\dot{\varepsilon}}}^{1.004} \cdot {f_T}^{0.775} \\ f_0 = 13.55 \\ f_\varepsilon = 1.00222 + 0.02773\varepsilon - 0.48905\varepsilon^2 \\ f_{\dot{\varepsilon}} = \exp(1.47674 + 0.1943 \ln \dot{\varepsilon}) \\ f_T = \exp\left(-4.74286 + 6.03766 \times \frac{1\,000}{T}\right) \end{cases} \tag{31}$$

3.4. Verification of constitutive equation

In order to verify the developed modified parallel constitutive equation for Ti-6Al-4V alloy at elevated temperatures, a comparison between the experimental and predicted flow stress data is carried out in Fig. 11. As can be seen from Fig. 11, the predicted flow stress data can track the experimental data of Ti-6Al-4V alloy, and there is a good agreement between the experimental and predicted values in single β phase (Fig. 11e and f). However, under some processing conditions in α + β phase (for example, 1 073 K at 1 s^{-1} and 0.01 s^{-1}, 1 123 K at 0.1 s^{-1}, 1 173 K at 0.1 s^{-1} and 0.01 s^{-1}, and 1 223 K at 1 s^{-1}), an obvious variation between experimental and calculated flow stress data can be seen, as shown in Fig. 11a, b, c and d. These results lead us to believe that a modification is required to improve the predictability of the developed constitutive equation through the all deformation conditions.

Table 4. The values of f_0 and ω_j obtained by multivariate regression.

	f_0	ω_1	ω_2	ω_3
α + β phase	86.57	0.9799	1.006	0.996
Single β phase	13.55	1.312	1.004	0.775

3.5. Modification of the constitutive equation

It should be noted that in Fig. 6 and Fig. 7 the values of $\ln(\bar{\sigma}_{\dot{\varepsilon}})$ and $\ln(\bar{\sigma}_T)$ for α + β phase show some deviation. Therefore, some errors may be introduced due to the determination of the values of $\ln(\bar{\sigma}_{\dot{\varepsilon}})$ and $\ln(\bar{\sigma}_T)$ by using linear fitting, finally affecting the accuracy of the constitutive equation. Therefore, a cubic fit and a parabolic fit are used to express $\ln(\bar{\sigma}_{\dot{\varepsilon}})$ and $\ln(\bar{\sigma}_T)$ as follows:

$$\ln(\bar{\sigma}_{\dot{\varepsilon}}) = 5.22067 + 0.15786 \ln \dot{\varepsilon} + 0.01589(\ln \dot{\varepsilon})^2 + 0.00275(\ln \dot{\varepsilon})^3 \tag{32}$$

$$\ln(\bar{\sigma}_T) = -46.25625 + 104.4418 \times \frac{1\,000}{T} - 52.90536 \times \left(\frac{1\,000}{T}\right)^2 \tag{33}$$

Then the formula of $f_{\dot{\varepsilon}}$ and f_T can be derived as follows:

$$f_{\dot{\varepsilon}} = \exp(1.48946 + 0.15785 \ln \dot{\varepsilon} + 0.01589(\ln \dot{\varepsilon})^2 + 0.00275(\ln \dot{\varepsilon})^3) \tag{34}$$

$$f_T = \exp\left(-51.37311 + 104.41592 \times \frac{1\,000}{T} - 52.89092 \times \left(\frac{1\,000}{T}\right)^2\right) \tag{35}$$

Thereafter, through the multivariate regression test, the modified values of f_0 and ω_j for α + β phase of Ti-6Al-4V alloy are obtained, as shown in Table 5.

Therefore, the developed constitutive equation of Ti-6Al-4V alloy for α + β phase is summarized on the bottom of this page.

$$\begin{cases} \sigma = f_0 \cdot {f_\varepsilon}^{0.980} \cdot {f_{\dot{\varepsilon}}}^{1.005} \cdot {f_T}^{0.990} \\ f_0 = 74.37 \\ f_\varepsilon = 1.04448 - 0.4447\varepsilon \\ f_{\dot{\varepsilon}} = \exp(1.48946 + 0.15785 \ln \dot{\varepsilon} + 0.01589(\ln \dot{\varepsilon})^2 + 0.00275(\ln \dot{\varepsilon})^3) \\ f_T = \exp\left(-51.37311 + 104.41592 \times \frac{1\,000}{T} - 52.89092 \times \left(\frac{1\,000}{T}\right)^2\right) \end{cases} \tag{36}$$

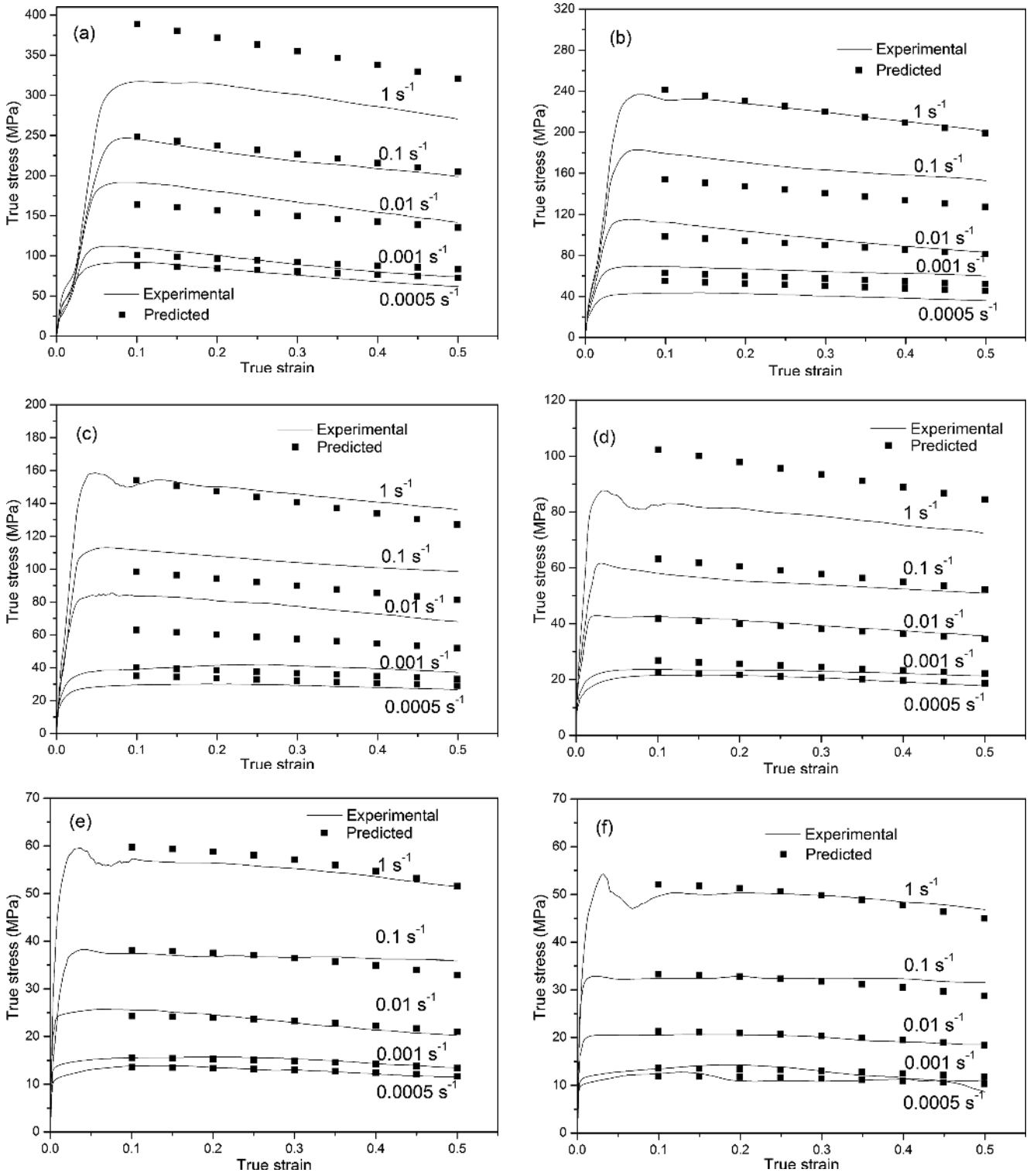

Fig. 11. Comparison of the experimental and predicted values by the modified parallel constitutive equation at temperatures of: (a) 1 073 K; (b) 1 123 K; (c) 1 173 K; (d) 1 223 K; (e) 1 273 K; and (f) 1 323 K.

3.6. Verification of the modified developed constitutive equations

The predictability of the modified constitutive equation in $\alpha + \beta$ phase is assessed by comparing the experimental and predicted data, as shown in Fig. 12. It can be seen that the predicted flow stress values from the modified constitutive equation track the experimental data throughout the entire deformation conditions. Only under one processing condition (i. e. at 1 123 K in 0.01 s^{-1}), can some variation between experimental and predicted flow stress data be observed (Fig. 12b).

The predictability of the developed constitutive equation is quantified in terms of standard statistical parameters such as correlation coefficient (R) and average absolute relative error ($AARE$). These are expressed as follows [51]:

Table 5. The modified values of f_0 and ω_j obtained by multivariate linear regression.

	f_0	ω_1	ω_2	ω_3
α + β phase	74.37	0.980	1.005	0.990

$$R = \frac{\sum_{i=1}^{C}(E_i - \bar{E})(P_i - \bar{P})}{\sqrt{\sum_{i=1}^{C}(E_i - \bar{E})^2 \sum_{i=1}^{C}(P_i - \bar{P})^2}} \tag{37}$$

$$AARE = \frac{1}{C}\sum_{i=1}^{C}\left|\frac{E_i - P_i}{E_i}\right| \times 100 \tag{38}$$

where E is the experimental flow stress and P is the predicted flow stress obtained from the developed constitutive equation. $\bar{E}$ and $\bar{P}$ are the mean values of E and P respectively. C is the total number of data points employed in this research. R is a commonly employed statistical parameter and provides information on the strength of the linear relationship between the experimental and predicted data. *AARE* is acquired through a term by term comparison of the relative error, and is an unbiased statistical parameter for determining the predictability of the developed constitutive equation. The correlation between experimental flow stresses and predicted data is given in Fig. 13. It can be seen that most of the data points are located close to the fitting lines, and the values of R and *AARE* are found to be 0.997 and 5.24 % respectively, which indicate that the modified parallel constitutive equation can give an accurate and precise estimate of the flow stress of Ti-6Al-4V alloy.

3.7. Comparison with other constitutive models

The accuracy of the proposed constitutive equation is evaluated by comparing with the original parallel constitutive model (OPCM), strain-compensated Arrhenius-type constitutive model (SACM) and DMNR.

The Arrhenius-type constitutive equation can be expressed in the following form:

$$\sigma = \frac{1}{\alpha}\ln\left\{\left(\frac{Z}{A}\right)^{1/n} + \left[\left(\frac{Z}{A}\right)^{2/n} + 1\right]^{1/2}\right\} \tag{39}$$

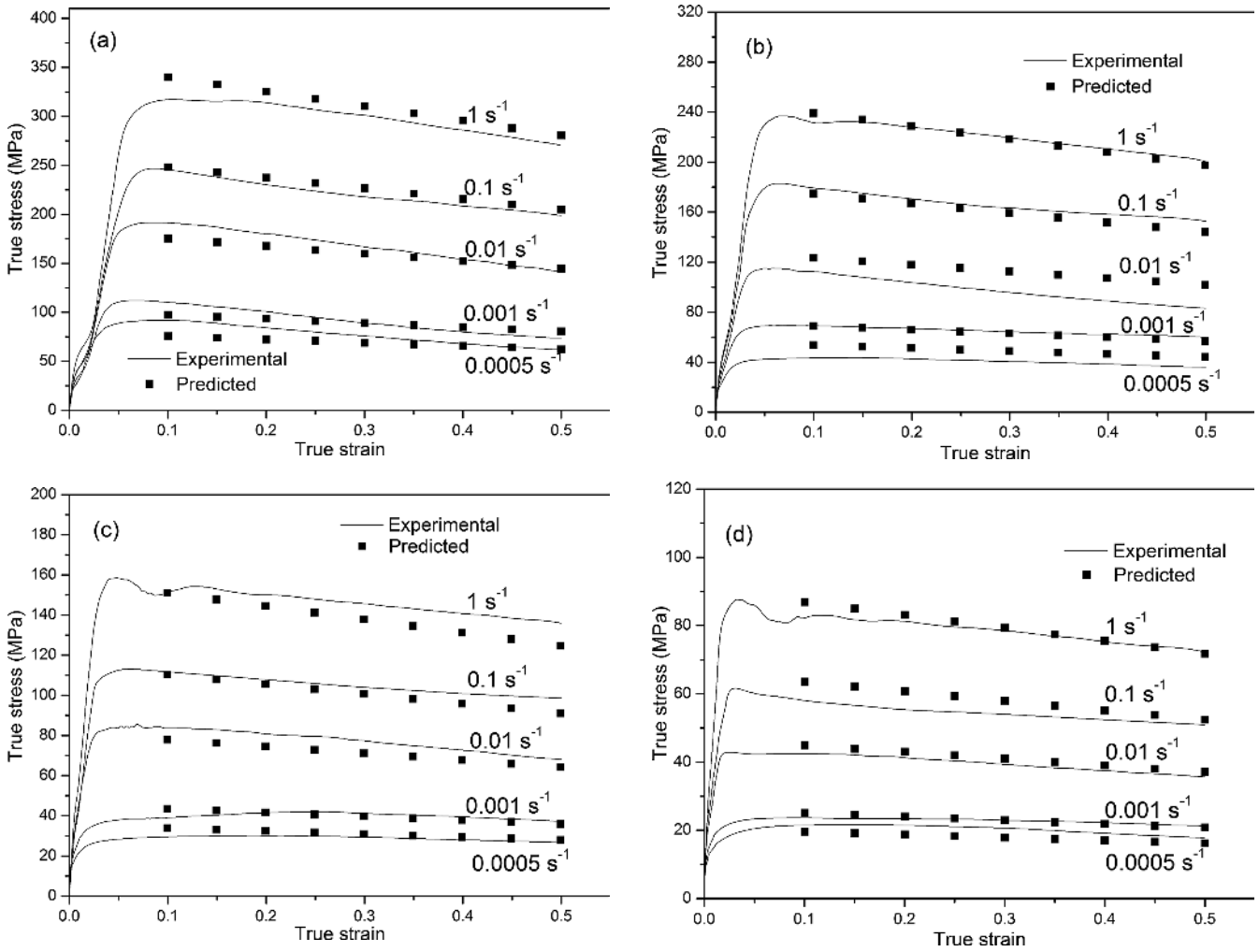

Fig. 12. Comparison between the experimental and predicted flow stress from the constitutive equation (considering the modification by temperature and strain rate) at temperatures of: (a) 1 073 K; (b) 1 123 K; (c) 1 173 K; and (d) 1 223 K.

where A, α and n are materials constants, and Z is the Zener–Holloman parameter, expressed as:

$$Z = \dot{\varepsilon} \exp\left(\frac{Q}{RT}\right)$$

The influence of strain on the Arrhenius-type constitutive equation is incorporated by assuming that the material constants (i.e. α, n, Q and ln$A$) are polynomial functions of strains, shown in Eq. (40), Table 6 and Table 7 [52]:

$$\begin{aligned} \alpha &= C_0 + C_1\varepsilon + C_2\varepsilon^2 + C_3\varepsilon^3 + C_4\varepsilon^4 + C_5\varepsilon^5 \\ n &= D_0 + D_1\varepsilon + D_2\varepsilon^2 + D_3\varepsilon^3 + D_4\varepsilon^4 + D_5\varepsilon^5 \\ Q &= E_0 + E_1\varepsilon + E_2\varepsilon^2 + E_3\varepsilon^3 + E_4\varepsilon^4 + E_5\varepsilon^5 \\ \ln A &= F_0 + F_1\varepsilon + F_2\varepsilon^2 + F_3\varepsilon^3 + F_4\varepsilon^4 + F_5\varepsilon^5 \end{aligned} \quad (40)$$

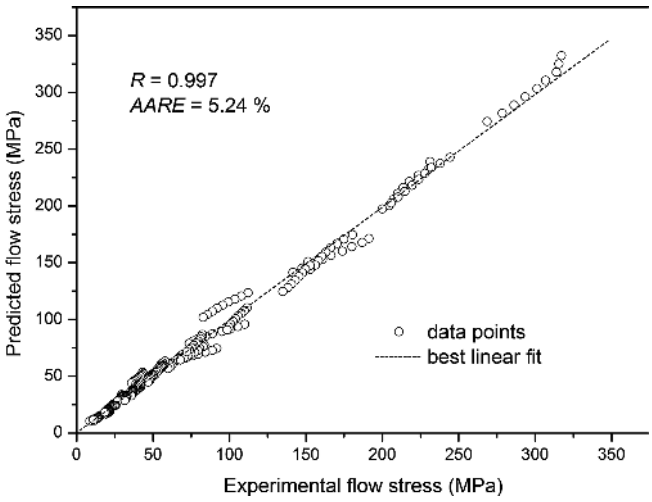

Fig. 13. Correlation between the experimental and predicted flow stress values.

The DMNR constitutive model is expressed as:

$$\begin{aligned} \ln\sigma = \ln A + a\ln f_{\varepsilon} + b\ln f_{\dot{\varepsilon}} + c\ln f_T \\ + d\ln f_{\varepsilon-T} + e\ln f_{\dot{\varepsilon}-T} + f\ln f_{\varepsilon-\dot{\varepsilon}} \end{aligned} \quad (41)$$

The values of converged weights (i.e. A, a, b, c, d, e, and f) are given in Table 8 [18].

Figure 14 illustrates the correlation between the experimental and predicted flow stress data from the OPCM, SACM and DMNR. The values of R for the OPCM, SACM and DMNR are 0.984, 0.994 and 0.985 respectively, which are all lower than that of the MPCM (0.997). Meanwhile, the values of *AARE* for the OPCM, SACM and DMNR are 8.72 %, 9.01 % and 10.97 % respectively, which are much higher than that of the MPCM (5.24 %). It should be noted that the value of *AARE* for DMNR is higher than that for OPCM. This may be due to the fact that the material constants of OPCM are obtained separately for α + β phase and single β phase. However, the material constants of DMNR are calculated without distinguishing α + β phase and single β phase.

As was mentioned above, a lot of hot forming processes for Ti-6Al-4V alloy are conducted on α + β phase. Therefore, the accuracy of the constitutive equation for Ti-6Al-4V alloy in the α + β phase region is more important than that in single β phase region. Table 9 gives the distribution of *AARE* for different constitutive models in α + β phase and single β phase. It can be seen from Table 9 that the value of *AARE* for MPCD in α + β phase is 6.29 %, while the values of *AARE* for other three models are all higher than 10 %. Meanwhile, the value of *AARE* for MPCD in single β phase is only 3.14 %, which is also lower than the values of other three models.

Moreover, the performance of the four constitutive models is further investigated by statistical analysis of the relative error. The predictions are compared with the corre-

Table 6. Coefficients of the polynomial for α + β phase.

α	n	Q	ln$A$
$C_0 = 0.01005$	$D_0 = 3.767$	$E_0 = 558.54$	$F_0 = 54.39$
$C_1 = -0.00454$	$D_1 = -0.6117$	$E_1 = -109.32$	$F_1 = -12.72$
$C_2 = 0.0234$	$D_2 = 7.842$	$E_2 = -518.04$	$F_2 = -49.69$
$C_3 = -0.0175$	$D_3 = -31.67$	$E_3 = 716.91$	$F_3 = 71.08$
	$D_4 = 39.71$		
	$D_5 = -11.05$		

Table 7. Coefficients of the polynomial for β phase.

α	n	Q	ln$A$
$C_0 = 0.0403$	$D_0 = 2.53$	$E_0 = 357.71$	$F_0 = 28.46$
$C_1 = -0.0941$	$D_1 = 32.41$	$E_1 = -1\,845.63$	$F_1 = -172.38$
$C_2 = 0.685$	$D_2 = -250.34$	$E_2 = 5\,149.8$	$F_2 = 479.35$
$C_3 = -2.104$	$D_3 = 857.79$	$E_3 = 11\,465.57$	$F_3 = 1\,082.48$
$C_4 = 2.970$	$D_4 = -1\,363.80$	$E_4 = -70\,104.05$	$F_4 = -6\,560.54$
$C_5 = -1.469$	$D_5 = 812.24$	$E_5 = 77\,725.09$	$F_5 = 7\,257.49$

Table 8. The values of converged weights in Eq. (41).

A	*a*	*b*	*c*	*d*	*e*	*f*
0.001316	0.385	0.138	1.062	–0.205	0.188	0.167

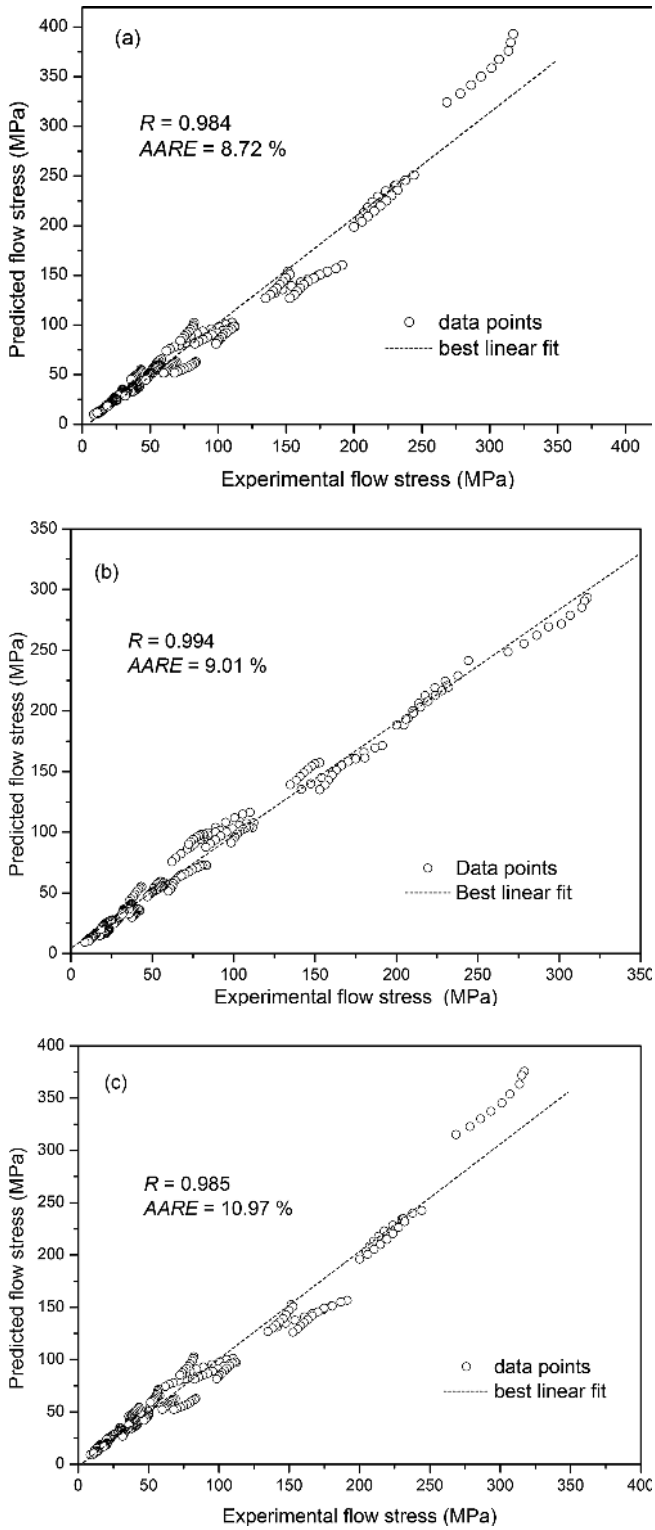

Fig. 14. Correlation between the experimental and predicted flow stress data from: (a) OPCM; (b) SACM; and (c) DMNR.

Table 9. The values of *AARE* (%) for different constitutive models.

constitutive model	α + β phase	single β phase	total
MPCD	6.29	3.14	5.24
OPCD	11.18	3.79	8.72
SACM	11.83	6.10	9.01
DMRN	10.97	10.97	10.97

sponding experimental data, and subsequently the relative errors are expressed as follows [53]:

$$\text{relative error} = \left(\frac{E_i - P_i}{E_i}\right) \times 100\ \% \tag{42}$$

The results of relative error are represented graphically as a typical number versus error plot, as shown in Fig. 15. As can be seen from Fig. 15, the relative errors of MPCM exhibit Gaussian distribution, and vary from –23.66 % to 18.96 %. The mean value of the relative errors for MPCM is only 0.00263. However, the relative errors vary from –29.82 % to 24.96 %, –27.56 % to 24.33 % and –27.25 % to 26.13 % for OPCM, SACM and DMNR respectively. Meanwhile, the mean values of the relative errors for OPCM, SACM and DMNR are –0.0199, –0.00778 and –0.017 respectively. Moreover, the number of relative errors in the range of –5 to 5 % for MPCM is more than that of the other three models. Therefore, the modified parallel constitutive equation based on multiple regression gives an accurate and precise estimate of the flow stress of Ti-6Al-4V alloy. Moreover, it should be noted that OPCM has been successfully applied to describe the flow behavior of Ti-NiNb alloy (*AARE* 8.78 % for as-cast and 7.95 % for as-forged TiNiNb alloy) [17] and Ti17 titanium alloy (*AARE* 8.26 %) [54]. Therefore, MPCM can also predict the flow stress of other materials rather than Ti-6Al-4V alloy accurately because MPCM is modified from OPCM. However, whether the accuracy of MPCM is higher than that of SACM and DMNR or not for other material is still unknown for us. Meanwhile, commonly used constitutive models (such as modified Johnson–Cook, modified Zerilli–Armstrong, and SACM) can be applied for both compression and tensile deformation of metal materials such as Ti-6Al-4V alloy [12], Al–Zn–Mg–Cu alloy [55], pure molybdenum [56], and so on. Therefore, MPCM may also be employed in numerical simulation with complex deformation (both compress and tension). Further research needs to be done to draw a firm conclusion.

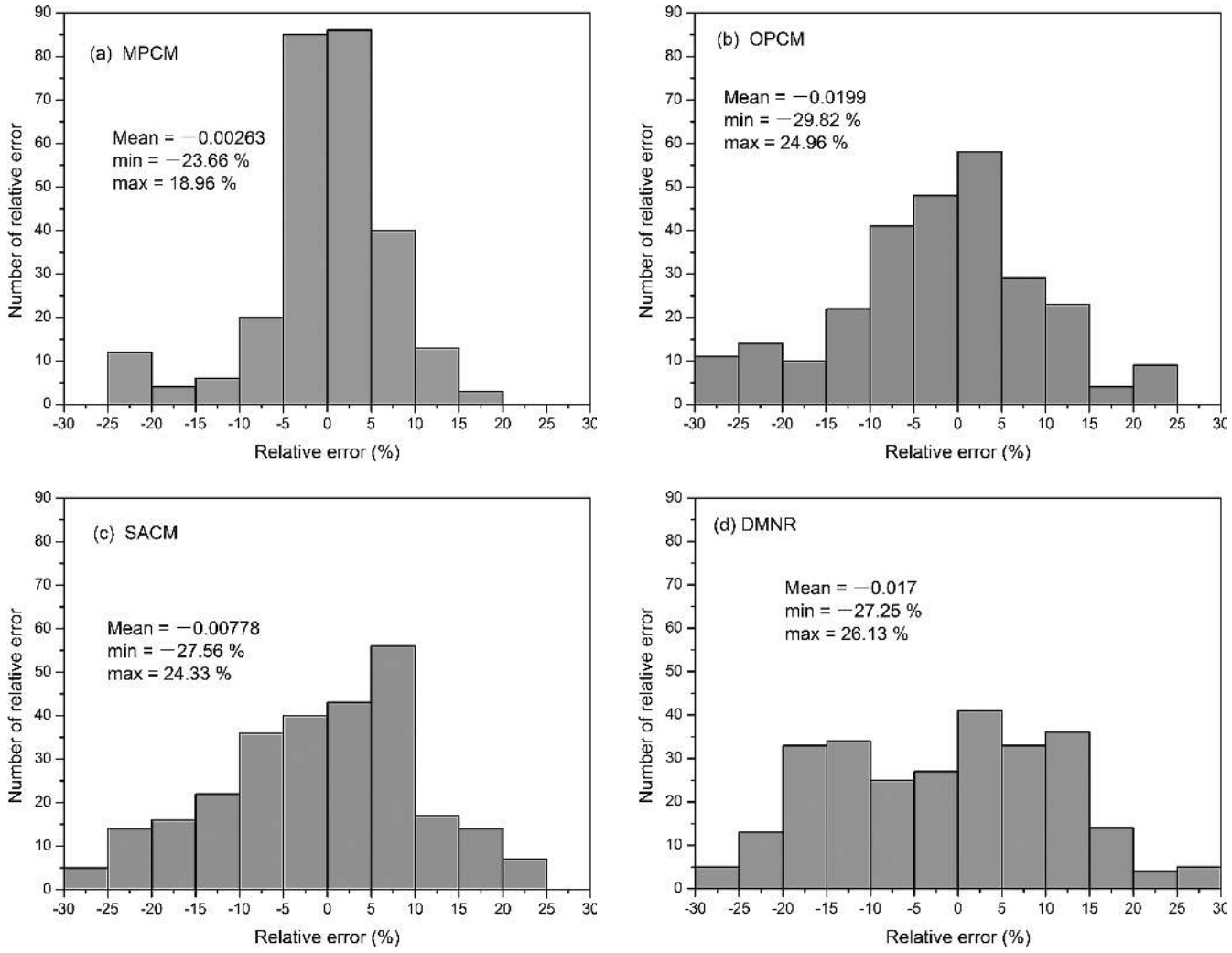

Fig. 15. Statistical analysis of the relative error by (a) MPCM; (b) OPCM; (c) SACM; and (d) DMNR.

4. Conclusions

A modified parallel constitutive equation based on multiple regression for Ti-6Al-4V alloy was developed by performing hot compression tests over a wide range of temperatures (1 073 – 1 323 K) and strain rates (0.0005 – 1 s^{-1}). Based on this study, following conclusions may be drawn:

1. A modified parallel constitutive equation was proposed to predict the high temperature flow behavior of Ti-6Al-4V alloy by taking into account the effects of strain, strain rate and deformation temperature on the flow stress.
2. The developed constitutive equation was verified by comparing the experimental and the predicted flow stress, and the predictability of the constitutive equation was evaluated by correlation coefficient and average absolute relative error. The results indicate that the modified parallel constitutive equation gives an accurate and precise estimate of the flow stress for Ti-6Al-4V alloy.
3. The predictability of the modified parallel constitutive equation was comparable to that of the original parallel constitutive model, strain-compensated Arrhenius-type constitutive model and double multiple nonlinear regression method. The result showed that the modified parallel constitutive equation shows a relatively higher accuracy than the other three constitutive equations.

The authors gratefully acknowledge the financial support received from Innovation Foundation of Western Materials (XBCL-3-19), Planned Scientific Research Project of Education Department of Shaanxi Provincial Government (15JS056), Industrial Science and Technique Key Project of Shaanxi Province (2016GY-207), Project of International Cooperation and Exchange of Shaanxi Provincial (2016 KW-054).

References

[1] J. Luo, M.Q. Li, H. Li, W.X. Yu: Mater. Sci. Eng. A 505 (2009) 88. DOI:10.1016/j.msea.2008.11.001
[2] F.Z. Wang, J. Zhao, N.B. Zhu: J. Mater. Eng. Perform. 25 (2016) 4875. DOI:10.1007/s11665-016-2337-4
[3] G. Chen, C.Z. Ren, X.D. Qin, J. Li: Mater. Des. 83 (2015) 598. DOI:10.1016/j.matdes.2015.06.048
[4] F. Weng, H.J. Yu, C.Z. Chen, J.L. Liu, L.J. Zhao, J.J. Dai, Z.H. Zhao: J. Alloys Compd. 692 (2017) 989. DOI:10.1016/j.jallcom.2016.09.071
[5] A. Ducato, L. Fratini, F. Micari: Proc. Inst. Mech. Eng., Part L: J. Mater. Des. Appl. 228 (2014) 154. DOI:10.1177/1464420713477344

[6] M. Abdulwahab, O. Enechukwu, V.S. Aigbodion, S.A. Yaro: J. Fail. Anal. Prev. 15 (2015) 952. DOI:10.1007/s11668-015-0042-5
[7] S. Bahl, S. Raj, S. Vanamali, S. Suwas, K. Chatterjee: Mater. Technol. 29 (2014) 64. DOI:10.1179/1753555713Y.0000000118
[8] F.Z. Wang, J. Zhao, N.B. Zhu, Z.L. Li: J. Alloys Compd. 633 (2015) 220. DOI:10.1016/j.jallcom.2015.01.284
[9] D. Yang, Z.Q. Liu: Materials 9 (2016) 1. DOI:10.3390/ma9080628
[10] L.X. Li, B. Ye, S. Liu, S.D. Hu, H.Q. Liao: J. Mater. Eng. Peform. 25 (2016) 4581. DOI:10.1007/s11665-016-2302-2
[11] Y. Sun, W.H. Ye, L.X. Hu: J. Mater. Eng. Perform. 25 (2016) 1621. DOI:10.1007/s11665-016-1988-5
[12] N. Kotkunde, H.N. Krishnamurthy, P. Puranik, A.K. Gupta, S.K. Singh: Mater. Des. 54 (2014) 96. DOI:10.1016/j.matdes.2013.08.006
[13] J. Luo, M.Q. Li, X.L. Li, Y.P. Shi: Mech. Mater. 42 (2010) 157. DOI:10.1016/j.mechmat.2009.10.004
[14] T.J. Luo, M.Q. Li, W.X. Yu: Mater. Des. 31 (2010) 3078. 2010.01.005. DOI:10.1016/j.matdes
[15] R. Picu, A.Majorell: Mater. Sci. Eng. A 326 (2002) 306. 5093 (01)01508 – 8. DOI:10.1016/S0921-
[16] C. Zhang, X.Q. Li, D.S. Li, C.H. Jin, J.J. Xiao: Trans. Nonferrous. Met. Soc. China 22 (2012) 457. DOI:10.1016/S1003-6326(12)61746-4
[17] M.L. Xiao, F.G. Li, W. Zhao, G.L. Yang: Mater. Des. 35 (2012) 184. DOI:10.1016/j.matdes.2011.09.044
[18] Z.W. Yuan, F.G. Li, H.J. Qiao, M.L. Xiao, J. Cai, J. Li: Mater. Sci. Eng. A 578 (2013) 260. DOI:10.1016/j.msea.2013.04.091
[19] D. Samantaray, S. Mandal, A.K. Bhaduri: Comput. Mater. Sci. 47 (2009) 568. DOI:10.1016/j.commatsci.2009.09.025
[20] T. Wang, H.Z. Guo, Y.W. Wang, Z.K. Yao: Mater. Sci. Eng. A 528 (2010) 736. DOI:10.1016/j.msea.2010.09.091
[21] M.H. Ghavam, M. Morakabati, S.M. Abbasi, H. Badri: Trans. Nonferrous. Met. Soc. China 25 (2015) 748. DOI:10.1016/S1003-6326(15)63660-3
[22] S.D. Sun, Y.Y. Zong, D.B. Shan, B. Guo: Trans. Nonferrous. Met. Soc. China 20 (2010) 2181. DOI:10.1016/S1003 – 6326(09)60439 – 8
[23] Z.G. Liu, P.J. Li, L.T. Xiong, T.Y. Liu, L.J. He: Mater. Sci. Eng. A 680 (2017) 259. DOI:10.1016/j.msea.2016.10.095
[24] V. Velay, H. Matsumoto, V. Vidal, A. Chiba: Int. J. Mech. Sci. 108 – 109 (2016) 1. DOI:10.1016/j.ijmecsci.2016.01.024
[25] G. Giuliano: Mater. Des. 26 (2005) 373. DOI:10.1016/j.matdes.2004.06.005
[26] G.C. Wang, M.W. Fu: J. Mater. Process. Technol. 192 – 193 (2007) 555. DOI:10.1016/j.jmatprotec.2007.04.059
[27] Z.L. Zhao, H.Z. Guo, L. Chen, Z.K. Yao: Rare Met. 28 (2009) 523. DOI:10.1007/s12598-009-0101-8
[28] X.M. Zhang, L.L. Cao, Y.Q. Zhao, Y.N. Chen, X.D. Tian, J.L. Deng: Mater. Sci. Eng. A 560 (2013) 700. DOI:10.1016/j.msea.2012.10.016
[29] S. Ghosh, G.S. Murty, S. Bhargava: Mater. Sci. Technol. 20 (2004) 1035. DOI:10.1179/026708304225019858
[30] T. Seshacharyulu, S.C. Medeiros, W.G. Frazier, Y.V.R.K. Prasad: Mater. Sci. Eng. A 284 (2000) 184. DOI:10.1016/S0921-5093(00)00741-3
[31] P.D. Nicolaou, S.L. Semiatin: Metall. Mater. Trans. A 36 (2005) 1567. DOI:10.1007/s11661-005-0248-3
[32] R.G. Guan, Y.T. Je, Y. Zhan, C.S. Lee: Mater. Des. 36 (2012) 796. DOI:10.1016/j.matdes.2011.11.057
[33] W.X. Yu, M.Q. Li, J. Luo: Rare Met. 31 (2012) 7. DOI:10.1007/s12598-012-0452-4
[34] P. Cantiello,B.D. Martino,F. Moscato: Mater. Sci. Eng. A 561 (2013) 17. DOI:10.1016/j.msea.2012.10.056
[35] G.A Salishchev, R.M. Galeyev, O.R. Valiakhmetov, R.V. Safiullin, R.Y. Lutfullin, O.N. Senkov, O.A. Kaibyshev: J. Mater. Process. Technol. 116 (2001) 265. DOI:10.1016/S0924-0136(01)01037-8
[36] P. Comley: J. Mater. Eng. Perform. 16 (2007) 150. DOI:10.1007/s11665-007-9025-3
[37] J. Luo, L. Li, M.Q. Li: Mater. Sci. Eng. A 606 (2014) 165. 2014.03.103. DOI:10.1016/j.msea
[38] Y.C. Zhu, W.D. Zeng, F. Feng, Y. Sun, Y.F. Han, Y.G. Zhou: Mater. Sci. Eng. A 528 (2011) 1757. DOI:10.1016/j.msea.2010.11.015
[39] Y.C. Zhu, W.D. Zeng, Y. Sun, F. Feng, Y.F. Han: Comput. Mater. Sci. 50 (2011) 1785. DOI:10.1016/j.commatsci.2011.01.015
[40] X.M. Yang, H.Z. Guo, H.Q. Liang, Z.K. Yao, S.C. Yuan: J. Mater. Eng. Peform. 25 (2016) 1347. DOI:10.1007/s11665-016-1963-1
[41] W.D. Zeng, Y. Shu, X.M. Zhang, Y.G. Zhou, Y.Q. Zhao, H. Wu, Y. Dai, J. Yang, L. Zhou: Mater. Sci. Technol. 24 (2008) 1222. DOI:10.1179/174328407X185884
[42] R. Ding, Z.X. Guo, A. Wilson: Mater. Sci. Eng. A 327 (2002) 233. DOI:10.1016/S0921-5093(01)01531-3
[43] A. Galiyev, R. Kaibyshev, G. Gottstein: Acta Mater. 49 (2001) 1199. DOI:10.1016/S1359-6454(01)00020-9
[44] Y.Q. Ning, B.C. Xie, H.Q. Liang, H. Li, X.M. Yang, H.Z. Guo: Mater. Des. 71 (2015) 68. DOI:10.1016/j.matdes.2015.01.009
[45] E.I. Galindo-Nava, P.E.J. Rivera-Dıaz-del-Castillo: Mater. Sci. Eng. A 543 (2012) 110. DOI:10.1016/j.msea.2012.02.055
[46] C. Shi, W. Mao, X.G. Chen: Mater. Sci. Eng. A 571 (2013) 83. DOI:10.1016/j.msea.2013.01.080
[47] P.M. Sargent, M.F. Ashby: Scr. Mater. 16 (1982) 1415. DOI:10.1016/0036-9748(82)90439-2
[48] J. Gao, M.Q. Li, G.J. Liu: Rare Met. 36 (2017) 86. DOI:10.1007/s12598-015-0660-9
[49] H.Q. Liang, Y. Nan, Y.Q. Ning, H. Li, J.Z. Zhang, Z.F. Shi, H.Z. Guo: J. Alloys Compd. 632 (2015) 478. DOI:10.1016/j.jallcom.2014.12.270
[50] P. Honarmandi, M. Aghaie-Khafri: Metallogr. Microstruct. Anal. 2 (2013) 13. DOI:10.1007/s13632-012-0052-6
[51] S. Mandal, P.V. Sivaprasad, S. Venugopal, K.P.N. Murthy: Appl. Soft. Comput. J. 9 (2009) 237. DOI:10.1016/j.asoc.2008.03.016
[52] J. Cai: PhD thesis, Study on preform design and forming process simulation for large-size frame forging of Ti-6Al-4V alloy, Northwestern Polytechnical University, Xi'an, Shaanxi, China (2011).
[53] H.Y. Li, X.F. Wang, D.D. Wei, J.D. Li, Y.H. Li: Mater. Sci. Eng. A 536 (2012) 216. DOI:10.1016/j.msea.2011.12.108
[54] J.L. Liu, W.D. Zeng, Y.J. Lai, Z.Q. Jia: Mater. Sci. Eng. A 597 (2014) 387. DOI:10.1016/j.msea.2013.12.076
[55] M. Zhou, Y.C. Lin, J. Deng, Y.Q. Jiang: Mater. Des. 59 (2014) 141. DOI:10.1016/j.matdes.2014.02.052
[56] B. Meng, M. Wan, X.D. Wu, Y.K. Zhou, C. Chang: Int. J. Refract. Met. Hard Mater. 45 (2014) 41. DOI:10.1016/j.ijrmhm.2014.03.005

(Received December 25, 2016; accepted March 20, 2017; online since May 29, 2017)

Correspondence address

Jun Cai
School of Metallurgical Engineering
Xi'an University of Architecture and Technology
No. 13 Yanta Road
Xi'an 710055
Shaanxi Province
P. R. China
Tel.: +86 13227772022
Fax: +86 02988202920
E-mail: jeffreycai0116@gmail.com
caijun@xauat.edu.cn

Bibliography
DOI 10.3139/146.111514
Int. J. Mater. Res. (formerly Z. Metallkd.)
108 (2017) 7; page 527 – 541
© Carl Hanser Verlag GmbH & Co. KG
ISSN 1862-5282